V–22 HIGH RATE OF DESCENT (HROD) TEST PROCEDURES AND LONG RECORD ANALYSIS

Albert Brand
abrand @bellhelicopter.textron.com
Principal Engineer, V–22 ITT

Ron Kisor
rkisor @bellhelicopter.textron.com
IPT L4 Leader V–22

Robert Blyth
rblyth @bellhelicopter.textron.com
Senior Engineer

Bell Helicopter Textron, Inc., Fort Worth, Texas

Dave Mason
david.h.mason @Boeing.com
Boeing V–22 IPT Lead, Flying Qualities

Chris Host
christian.t.host @boeing.com
Class IV UAV Prog. Manager, Future Combat Systems

The Boeing Company, Ridley Park, PA

ABSTRACT

In August 2003, the V–22 Integrated Test Team completed a thorough investigation of the V–22's low-speed / HROD flight characteristics. Testing defined an operational envelope for the aircraft and demonstrated flight regimes free from vortex ring state (VRS). Tests also probed deeply into fully developed VRS to determine precise flight conditions where it may be encountered, and to confirm the ability of the V–22 to recover from the condition. The ability to tilt the nacelles proved to be a powerful and (in every case) reliable means for rapidly regaining aerodynamic function of the rotors, even when operating in VRS beyond the point of having sufficient controllability. Results for steady-state HROD conditions are presented and the methods for testing are described. In an operational sense, the test results show that the V–22 has a significantly higher rate of descent margin for avoiding VRS with respect to the published NATOPS limitation than conventional low disk-loading helicopters. Furthermore, dynamic maneuver testing of the V–22 showed that VRS cannot be initiated outside the steady-state VRS boundary. Simple engineering analysis is used to show that the V–22's steady-state VRS boundary is predictable by simple methods that work for conventional helicopters. High blade twist, and the side-by-side rotor configuration of the V–22 do not play a significant role in defining the VRS boundary.

NOMENCLATURE

AFCS	automatic flight control system
C_T	rotor thrust coefficient, $\frac{T}{\rho\pi R^2 V_{TIP}{}^2}$
HROD	high rate of descent
IPW	inertia plus wind (velocity determination method)
ITT	Integrated Test Team
LAS_{VT}	LAS indicated total airspeed, kn
PFCS	primary flight control system
R	rotor radius, 19 ft
ROC	rate of climb, ft/min
T	rotor thrust, lb
TCL	thrust control lever (equivalent to collective in VTOL mode), in
UA_KT	forward airspeed determined by inertia plus wind method, kn
V_{Tip}	rotor blade hover tip speed, 790 ft/s
V_T	true airspeed determined by inertia plus wind method, kn
V_{T_LAS}	true airspeed determined by LAS, kn
V_{XLAS}	LAS indicated forward velocity, kn
V_x	forward speed, ft/s
V_z	descent speed, ft/s
VTOL	vertical takeoff and landing (V–22 Helicopter mode)
$v_{i\ hover}$	hover induced velocity, $V_{TIP}\sqrt{\frac{C_T}{2}}$
$\bar{\mu}_x$	forward speed normalized by hover induced velocity, $V_x/v_{i\ hover}$
$\bar{\mu}_z$	Descent speed normalized by hover induced velocity, $V_z/v_{i\ hover}$
$\bar{\lambda}_i$	Rotor induced velocity, normalized by hover induced velocity

INTRODUCTION

Vortex ring state (VRS) is an aerodynamic phenomenon. Its presence places operational restrictions on all rotorcraft because when it is encountered, the aircraft's controllability may be significantly degraded. In terms of simple momentum theory, rotor performance can be readily predicted if the wake has a well-defined slipstream. In hovering flight, the rotor wake is more-or-less confined to a stream tube beneath the rotor. Similarly, in autorotation, the rotor wake is above the rotor and the stream tube is again well defined. VRS,

Presented at the American Helicopter Society 60th Annual Forum, Baltimore, MD, June 7–10, 2004.

however, presents itself as a case where the wake trajectory cannot be categorized as a stream-tube. Simple, but formerly accurate, methods for predicting rotor thrust break down. Early experiments conducted by Drees in 1950 (Ref. 1) showed that the VRS wake flow pattern is chaotic, with transient flow spillage around the rotor disk, and significant wake flow reingestion through the rotor. A toroidal (or donut-like) flow pattern emerges around the rotor in VRS. Experiments conducted by Yaggy (Ref. 2) and Azuma (Ref.3) showed that VRS coincides with the onset of progressively larger thrust fluctuations for a range of descent rates and low forward speed. Although VRS is an important general limitation of rotor performance, Johnson's survey of VRS research (Ref. 4) shows that there have been relatively long dormant periods in this field of research.

In recent times, Betzina (Ref. 5) examined, for the first time, the characteristics of an experimental side-by-side proprotor configuration in descent conditions. The experiment was able to detect thrust fluctuations over a range of vertical and horizontal speeds in the VRS regime. For a fixed collective pitch, the experiment indicated that the mean thrust could be reduced by more than 25% during VRS. Conversely, a cross plot of test data showed that a relatively large collective pitch increase would be required to maintain thrust during deep VRS penetrations. For the same data, thrust fluctuations with three standard deviations as large as 50% of the mean thrust were measured.

Notable analytical treatments of VRS include the work of Wolkovitch (Ref. 6), Newman et al. (Ref. 7), and Taghizad et al. (Ref. 8), which utilize extensions of momentum theory as a theoretical basis for determining the VRS boundary in terms of forward speed and descent rate. Johnson (Ref. 4) also develops a VRS model from extensions to momentum theory applied to tiltrotors. Simple models for predicting the VRS boundary are of particular interest in the present paper, because the notion had been put forward that the V–22's high disk loading, high blade twist, and side-by-side rotor configuration would increase its susceptibility to VRS. It was suggested that simple engineering models that account only for the high disk loading would not properly capture the VRS boundary for the V–22. For this reason, the engineering model of Newman et al. (Ref. 7) is compared to V–22 test results later in this paper, appearing to capture the general vicinity of the VRS boundary for the V–22.

Results in the present paper relate primarily to the Phase I evaluation of the V–22's steady state VRS boundary. This boundary is determined when the aircraft descends at relatively constant, or "quasi-steady," conditions. While aircraft controllability was evaluated throughout this test phase, the aircraft maintained, as far as possible, a steady, trim attitude during testing. It had been asserted by some that even if the V–22 were operating safely outside of its steady state VRS boundary, VRS could be initiated on one or both rotors simply by the effect of yaw rate or roll rate. Since yaw rate would, in effect, reduce the forward speed of one rotor, it was speculated that, near the VRS boundary, the reduced forward speed could place the rotor inside the VRS boundary and loss of control would result. Speculation concerning roll rate was similar: the argument was that roll rate would cause one rotor to effectively descend faster, forcing that rotor into the (nearby) VRS boundary. Although the Phase I (steady state) control evaluations at the VRS boundary gave every indication that the steady-state, or static VRS boundary was in fact the most conservative boundary where VRS onset could be encountered, a second test phase evaluating dynamic maneuvers was also completed. In this second test phase, reported by Kisor et al. (Ref. 9), it was confirmed that rapid rolling, yawing, high pitch decelerations, and a host of multi-axis maneuvers, could not induce VRS outside the static VRS boundary. Tests showed that rotor control inputs and maneuvers suppressed VRS symptoms, allowing the aircraft to penetrate deep into the static VRS onset boundary and emerge from it without hindrance. In dynamic maneuver testing, VRS symptoms were detected only deep within the static VRS boundary when the descent angle exceeded 65 degrees.

Kisor et al. (Ref. 9) develops the V–22 static VRS boundary using thrust assessments and asymmetry criteria for numerous individual test records. The present paper utilizes a different (long record) approach to assess the location and severity of VRS. The technique (discussed later) pools contiguous streams of flight test data into a single, large, densely populated map for evaluating VRS criteria. The long-record analysis method provides independent confirmation of the V–22's static VRS boundary, consistent with the results of Kisor et al. in Ref. 9.

V–22 HROD INSTRUMENTATION & TESTING

The combination of testing at low forward speed and high rate of descent presented a unique challenge to the V–22 Integrated Test Team (ITT). Conventional rotorcraft airspeed systems rely on pitot-static systems that are unreliable at speeds below 30 knots. Even if the instrument's pressure transducer can be calibrated for low pressure differentials, the device remains subject to significant position error, because the static pressure in the vicinity of the rotor wake does not represent free-stream conditions. A boom-mounted ultrasonic anemometer was adapted for the V–22 to provide more accurate readings of velocity in the low-speed/high rate of descent (HROD) regime. As shown in Fig. 1, the low airspeed sensor (LAS) was located approximately 81 inches ahead of the nose. Preliminary evaluations by the ITT (Ref. 10) showed that the device could accurately measure flow

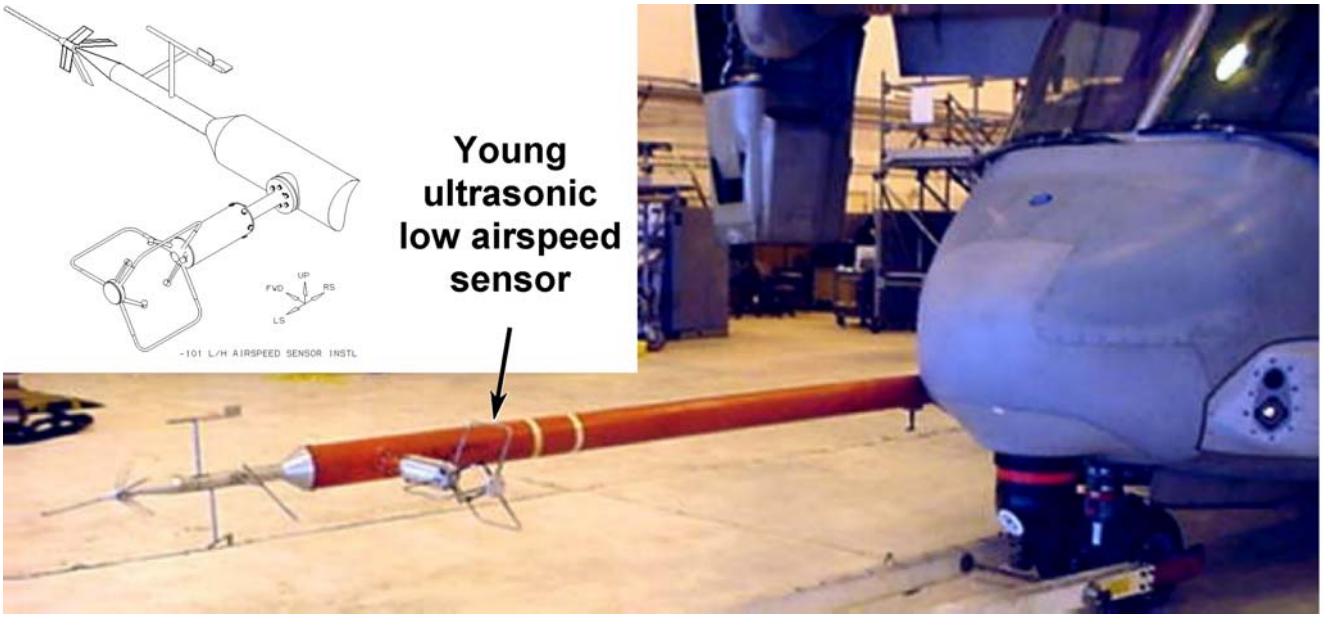

Fig. 1. V–22 HROD test aircraft with boom-mounted LAS and conventional angle of attack and sideslip, and airspeed flight test hardware.

velocity for the expected range of sideslip and high angle of attack. However, the relatively small distance from the nose did not completely eliminate position error. Subsequent flight test analysis indicated that the local velocity field (at the probe sensor) remained influenced by the airframe, and, in VRS conditions, the rotor wake completely dominated the sensor readings.

Due to the nature of testing, all low-speed/HROD flights were conducted at high altitudes, ranging from 3,000 ft to 9,000 ft (914 to 2,740 m). Testing utilized inertial (GPS-corrected) navigation, wind measurement, and considerable post-test analysis to arrive at final airspeed information for each descent. Since the testing was progressive in terms of approaching the VRS boundary, the LAS was calibrated concurrently with other test plan objectives. In-flight calibration of the low-airspeed sensor (LAS) allowed an understanding of the device to be developed in the course of testing. Its use was desired particularly for the 10–40 knot forward speed range, where the conventional airspeed system was not reliable. In approaching the VRS boundary, the LAS allowed the test team to target specific flight conditions for buildup and prevented inadvertent entry into undeveloped flight regimes. As the LAS behavior became well understood, its use by the pilots allowed deep penetrations into VRS and guided dynamic maneuvering into and beyond the VRS boundary.

INERTIA PLUS WIND TEST PROCEDURE

Prior to each day's test, a weather balloon was launched to assess winds aloft. Testing required steady winds, allowing only moderate velocity gradients with altitude. If the balloon data were deemed acceptable, testing proceeded, and the V–22 itself was used to more accurately determine the winds aloft. The V–22's flight control and avionics system software controls a suite of navigation and guidance systems. At any time, the aircraft position, attitude, ground speed, and attitude rates are available from the Lightweight Inertial Navigation System (LWINS). To conduct low-speed/HROD testing, and to simultaneously calibrate the LAS, a test procedure was developed to measure the winds aloft, and then use these winds with the measured ground speed to target the forward speed and rate of descent using on-board inertial reference velocities. The LAS calibration and the low speed/HROD testing hinged on the ability to determine a "known" true airspeed. By combining inertial reference velocities, and knowledge of the winds aloft, the aircraft true airspeed can be derived by summing the inertial velocity vector with the wind vector.[1]

The test procedure called for preceding each low forward speed descent with a "wind survey" climb over the test area. During a wind survey climb, the V–22 was operating in airplane mode at a specified airspeed and power setting where the conventional airspeed system was highly accurate. Under these conditions, the true airspeed vector (determined using the conventional airspeed system) was compared with

[1] Note that wind velocity is always defined by the direction from which it originates. This is opposite to the definition of most other vectors (such as aircraft velocity), which aim in the direction of destination. As a consequence, true airspeed is defined as inertial velocity plus wind velocity (IPW).

simultaneous readings of the aircraft inertial velocity based on an LWINS unit. The difference between the two velocities defined the wind aloft profile. Once the prevailing wind vector (direction and speed) was known, descent testing could be conducted exclusively by the inertial navigation system, accounting for the measured wind to achieve target airspeeds. The process is somewhat time-consuming, because long steady climbs in airplane mode are required at regular intervals between descents to keep wind data current. In actual testing, flight test engineers evaluated the wind survey data moments after each climb was completed. While pilots prepared the aircraft for helicopter (VTOL) mode descent, engineers utilized telemetry data to determine an altitude band where the measured wind speed and wind direction would be relatively constant for the descent. The aircraft was directed to a heading that provided a direct tailwind for the target altitude band. The average wind speed for the altitude band was added to the desired target air speed to arrive at the inertial reference speed used to guide the aircraft on each low forward speed descent profile.

WINDS ALOFT AND LONG RECORD POST-PROCESSING

Although the pilot was asked to target and hold a specific inertial speed throughout the test altitude band, variations in the wind profile had to be accounted for in assessing true airspeed and descent rates after the day's testing was complete. Post-processing software was developed to examine wind profile variations with altitude and time. During a descent through the test altitude band, winds could be expected to vary by $\pm$5 knots. Additionally, winds at a given altitude could vary over time, as determined by successive wind surveys. The approach was to correct the initial estimate of wind (used to target the descent) by interpolating between wind profiles obtained in successive "wind survey climbs." The wind interpolation scheme allowed a more accurate assessment to be made of the actual air speeds during descent, but required use of a contiguous data record that contained all the wind information associated with the descents in a single time history file. It was understood that estimated winds could be contaminated by gusts that occur during the descent, and that these gusts would be different from gusts seen during the climbs. It was also understood that winds would be based on climbs taken several minutes apart, and possibly in different regions of the test area. The resulting wind variability contributed to scatter in assessing the actual aircraft speed, but the preponderance of accumulated masses of data tend to level the effects of wind variability in an average sense and allowed an accurate LAS calibration to be made, independent of the conventional airspeed system. Final results for the LAS calibration were compared against the boom airspeed system, and showed that the instruments were generally within 2 knots of each other during non-HROD flight conditions.

Figure 2 shows a typical long record flight profile over the Atlantic Test Range near the Patuxent River Naval Air Station. The flight path corresponds to 79 minutes of contiguous test data from a December 2002 test. The thin (red) curve shows the 3-D flight path containing climbs, turns, and descents. The thick (blue) portions of the flight path represent HROD conditions, where the nacelles were configured for 95 degrees to maximize tip path plane angle of attack, landing gear was down, and flaperons were set to 72.5 degrees. The black trace underneath represents the corresponding ground track. The track indicates that nine low forward speed HROD descents were completed in this particular record. Altitude changes in the flight path also include eight wind survey climbs. To qualify as a wind survey, the climb had to be at a moderate rate (~2500 ft/min [~762 m/min]), and the aircraft had to be configured for airplane mode at 100% rotor speed, with an airspeed close to 170 kn. This configuration minimized the errors of the reference boom true airspeed.

The variation of wind speed for the entire flight of Fig. 2 is depicted in Fig. 3, where it is plotted as a function of altitude. The thin (blue) curves in Fig. 3 represent the known wind speed at the aircraft location as obtained during wind survey climbs. The thick black traces represent the "best estimate" of winds for all other flight segments, as interpolated by post processing the wind survey climbs, including wind conditions during descent tests. With the wind data available for all test conditions, the true reference airspeed is available in HROD segments by adding the wind vector to the inertial (GPS corrected) velocity. Thus, the aircraft true airspeed during descent is determined without relying on the conventional aircraft airspeed system.

HROD Envelope Results

The low-speed/HROD envelope was probed in numerous successive flights at decreasing forward speeds and increasing sink rates. Fig. 4 shows the range of forward speeds and rates of descent as determined using the inertia-plus-wind (IPW) method during the course of testing over several months. The data in Fig. 4 represent numerous contiguous (long) records of flight test data for times when the aircraft was in an appropriate VTOL mode HROD configuration. Each data point represents a ½ second time interval pulled from the contiguous data stream. For reference, the published V–22 NATOPS descent rate limitation is shown as the solid blue line. As stated earlier, these data represent only the test phase where steady rates of descent were targeted, and are referred to as static HROD conditions, used to define

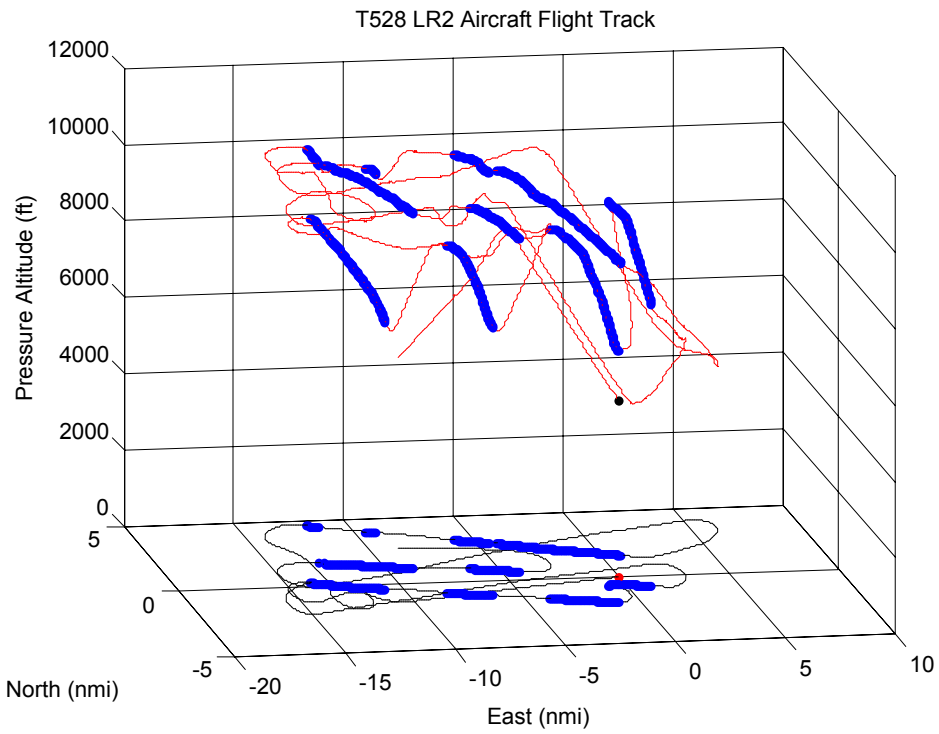

Fig. 2. **A typical long record flight path and ground track for HROD testing shows that descent data were acquired on a fixed heading (set with tail wind). Descents are interleaved with periodic wind survey climbs to acquire wind profiles.**

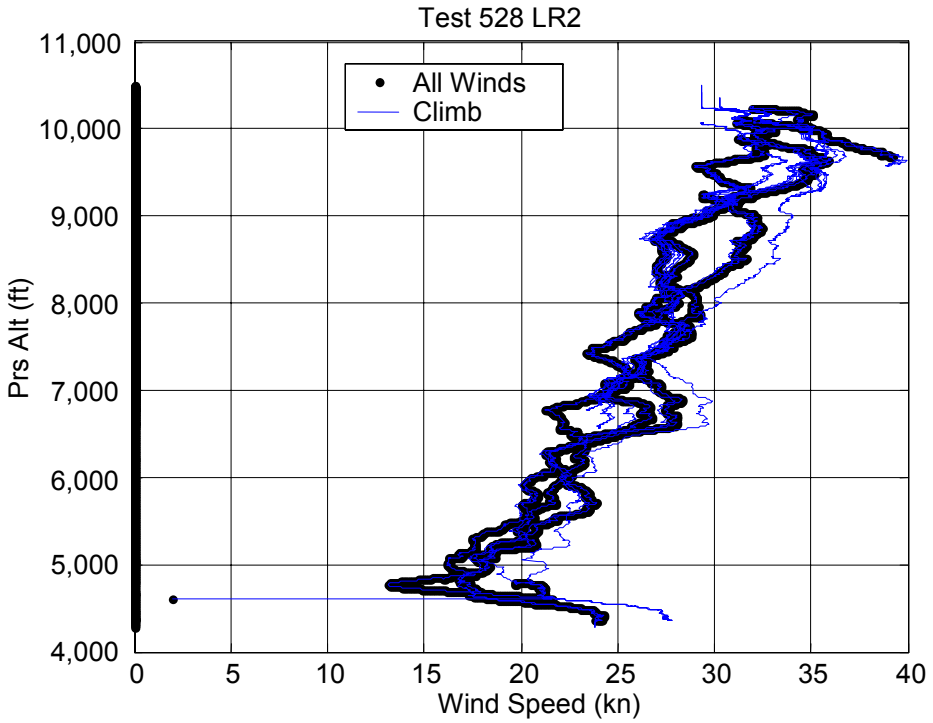

Fig. 3. **Wind speed/altitude profiles are obtained during climbs (when the basic air data system is "known accurate").**

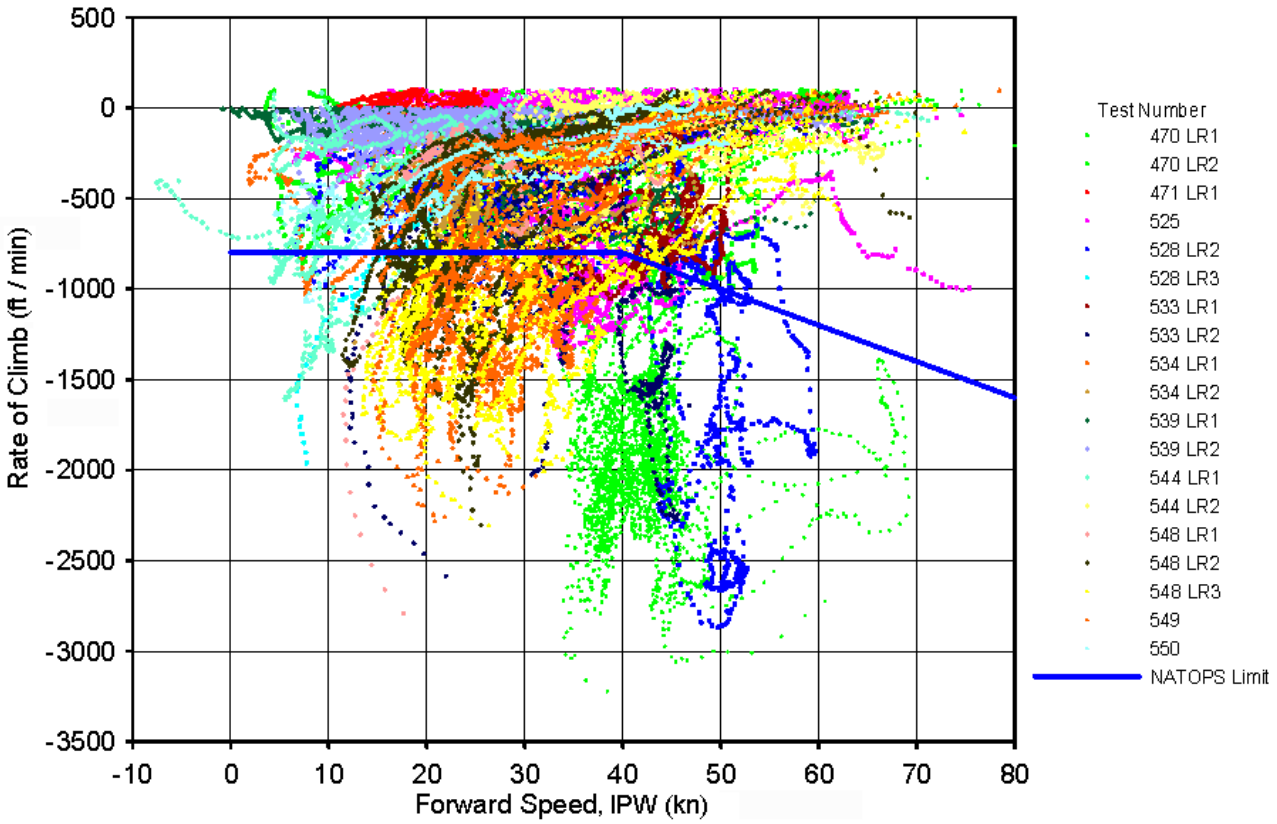

Fig. 4. V–22 HROD data from static VRS envelope testing. Each point on the chart represents a 1/2-second interval of flight test data.

the static VRS boundary. During this phase of testing, the controllability of the V–22 was continually assessed by first achieving the target forward speed, then descent rate, and then by applying and evaluating control inputs. In addition, the recovery from each descent provided continual demonstration that nacelle tilt would positively extricate the aircraft from all regions of the HROD envelope, including deep within the VRS region. The process allowed an orderly and predictable progression into unexplored regions of the HROD envelope.

Additional test points that explored dynamic maneuvers in HROD conditions are not shown in Fig. 4 because these points were not needed to define the static VRS boundary. In the course of testing it became readily apparent that dynamic maneuvers are much less restrictive than steady descents, as far as defining the VRS onset boundary. V–22 dynamic maneuver testing presented by Kisor et al. (Ref. 9) showed that the V–22 can accelerate through a region of the static HROD envelope, passing through rates of descent and forward speed that would cause fully developed VRS symptoms under steady-state descent conditions. The static VRS envelope thus represents the most conservative boundary for which VRS symptoms may be encountered. This result is indicative of the principle that VRS conditions take time to build up, a notion that led the ITT to investigate whether the onset of VRS symptoms could be delayed by introducing unsteady motions into the rotor system. As shown by Kisor et al. (Ref. 9), measurable VRS suppression could be achieved even with relatively small automatic inputs generated by the flight control system.

As mentioned previously, the static HROD flights included control evaluations consisting of control doublets and pulses of increasing amplitude as a buildup for deeper penetration into the static HROD envelope. Figure 4 shows that testing progressed well beyond the 800 ft/min descent rate limitation defined by the current V–22 NATOPS flight manual for VTOL mode descents below 40 kn. Various degrees of VRS symptoms were encountered as the test program attempted to detect control authority degradation and, ultimately, the limits where uncommanded roll (described later) could be expected. The data in Fig. 4 are a reflection of the buildup of test conditions. Many overlapping points are available at low rates of descent, because all test cases must first pass through low descent rates to achieve high descent rate. For rates of descent greater than 1000 ft/min, the amount of overlap diminishes. At 2000 ft/min and higher, only a few

traces extend below the "cloud" of points. These "low hanging" traces probed deeply into the vortex ring state. Indeed, several of these traces appear to terminate in space. A terminated trace at low-speed/HROD means that the aircraft was unable to maintain roll control and was reconfigured to recover from the condition. Upon loss of lateral control, the recovery technique called for rotating the nacelles forward (from the 95-degree test position) at maximum rate for 2 seconds (approximately 16 degrees of nacelle tilt change). When the nacelles tilted forward of 90 degrees, the point was no longer included in Fig. 4. In all cases, forward nacelle motion proved to be a powerful technique for clearing the rotor of VRS and provided almost immediate restoration of lateral control, allowing the aircraft to return to the top of the test altitude band for continued testing.

LOW AIRSPEED SENSOR BEHAVIOR

Based on initial test flights, it was determined that the LAS could be used to achieve the primary goal of safely expanding the HROD test envelope. The high altitude/low speed testing gave pilots poor visual cues regarding airspeed and sideslip. Therefore, in terms of targeting specific test conditions, the LAS proved to be an effective tool, particularly in the very low speed regime. Here, pilots were particularly concerned with preventing the possibility of rearward descending flight—an uncomfortable situation with respect to aircraft handling qualities. As more data were accumulated, the LAS behavior was continuously monitored so that any obvious limitations could be assessed.

The trend of LAS behavior for all contiguous records shown in Fig. 4 is given in Fig. 5, which presents the LAS total airspeed versus the "best estimate" total airspeed based on inertia plus wind (IPW). In Fig. 5 (and subsequent figures), the "inertia plus wind" total speed is denoted as V_T. It is clear that any given LAS total speed will correspond to a range of IPW total speeds with a scatter band of approximately $\pm$10 knots. It is presumed that the scatter in IPW speed (V_T) corresponds to uncertainty in the ability to accurately assess the (actual) winds during each descent. However, it is obvious that some data points (particularly in the V_T = 15 to 25 knot range) are well outside the $\pm$10 knot scatter band and cannot be attributed to wind variability. These "large scatter" data points are attributed to rates of descent near and beyond the VRS boundary.

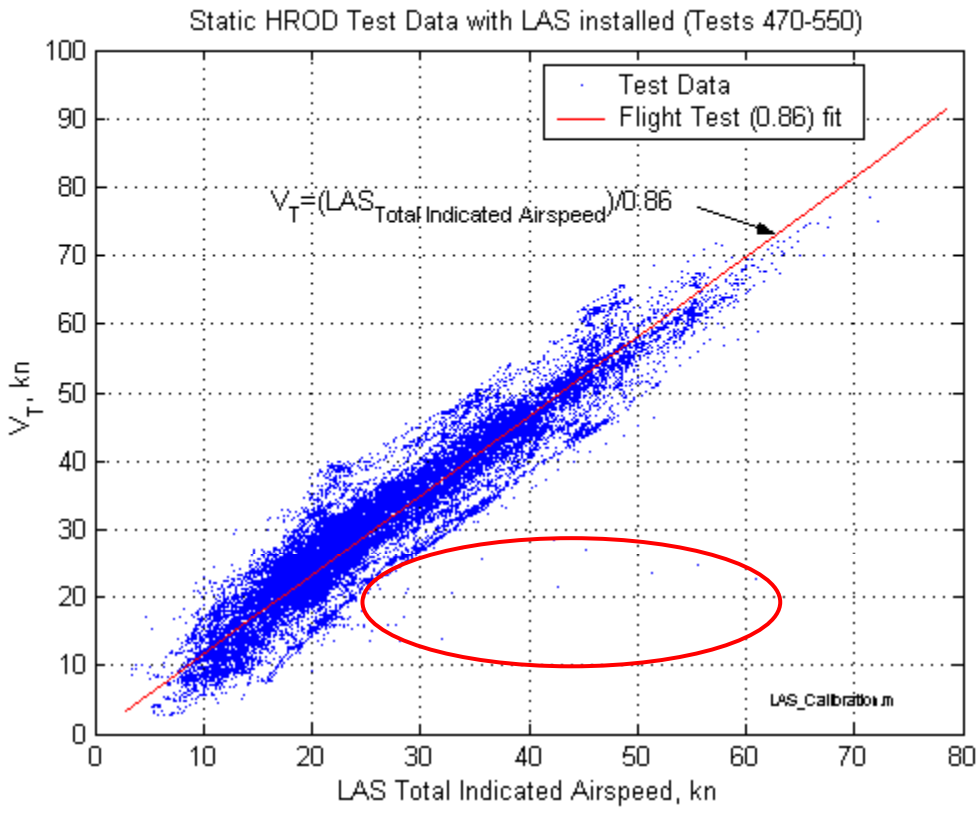

Fig. 5. For a given LAS total speed, a range of IPW total speed is contained in the database. Scatter in the circled data are attributed to VRS effects.

Initially, it was anticipated that the LAS indicated airspeed would be a function of the rotor wake skew angle, and the airframe angle of attack. Although the data of Fig. 5 covers a 70 kn airspeed range and angles of attack from 0 deg to 90 deg, the data are surprisingly linear. This is attributed to the relatively large separation distance between the LAS and the aircraft nose/rotors. Early testing showed that the LAS total indicated airspeed was approximately 86 percent of the free-stream total velocity throughout most of the descending flight envelope. The result indicates that the approaching flow tends to slow down as it nears the airframe and negotiates a path around it. Some of the scatter in Fig. 5 is, nevertheless, attributable to the effect of descent rate. The LAS behavior in Fig. 5 can be expressed three-dimensionally as a function of descent rate as shown in Figure 6, which constitutes a "best surface" fit to the LAS total airspeed over the range of descent rates. It is clear that the LAS total airspeed reading is fairly linear over much of the flight envelope, but at higher rates of descent, some nonlinear behavior is evident. When the rate of descent exceeds 2000 ft/min (610 m/min), and the true airspeed is below 40 knots, the LAS begins to see higher velocities than the linear trend. The nonlinear behavior is attributed to rotor wake effects in VRS conditions, as explained next.

AERODYNAMIC TRENDS AT THE VRS BOUNDARY

Because the LAS speed scales with total free-stream speed, the previous figures have dealt exclusively with total velocity. The static HROD testing, however, was based on targeting a forward speed component and a descent rate. As Kearney and Lake indicate in Ref. 10, the LAS can readily separate the total velocity into constituent components. The corresponding 3-D plot of horizontal LAS velocity (V_{XLAS}) versus IPW true horizontal speed (UA_KT) is shown in Fig. 7 and indicates that large negative V_{XLAS} readings occur when the forward speed is low and descent rate exceeds 2000 ft/min. This nonlinearity in V_{XLAS} is therefore the main culprit in the total airspeed nonlinearity of Fig. 6. It is directly attributable to vortex ring state effects, and coincided with pilot reports of the boom-mounted angle of attack vanes "going limp" or losing their directivity. The sudden appearance of a negative V_{XLAS} velocity indication in the cockpit was a cause of concern until its behavior could be explained. There was a strong desire to avoid rearward flight in unexplored portions of the descent flight envelope, and negative V_{XLAS} readings initially caused pilots to recover from the condition. The fact that V_{XLAS} was not linear with true horizontal speed (UA_KT) near the VRS boundary did not prevent its use in targeting a desired forward speed. By the time highly nonlinear portions of the calibration surface were encountered, the aircraft would already be encountering VRS symptoms, and target speeds could be evaluated by post processing the inertial reference velocity data to determine actual conditions.

During VRS, the negative V_{XLAS} signal indicates that the probe is encountering an outward-moving rotor wake flow. The LAS behavior in VRS is explained on the basis of flow patterns observed while hovering in ground effect (IGE).

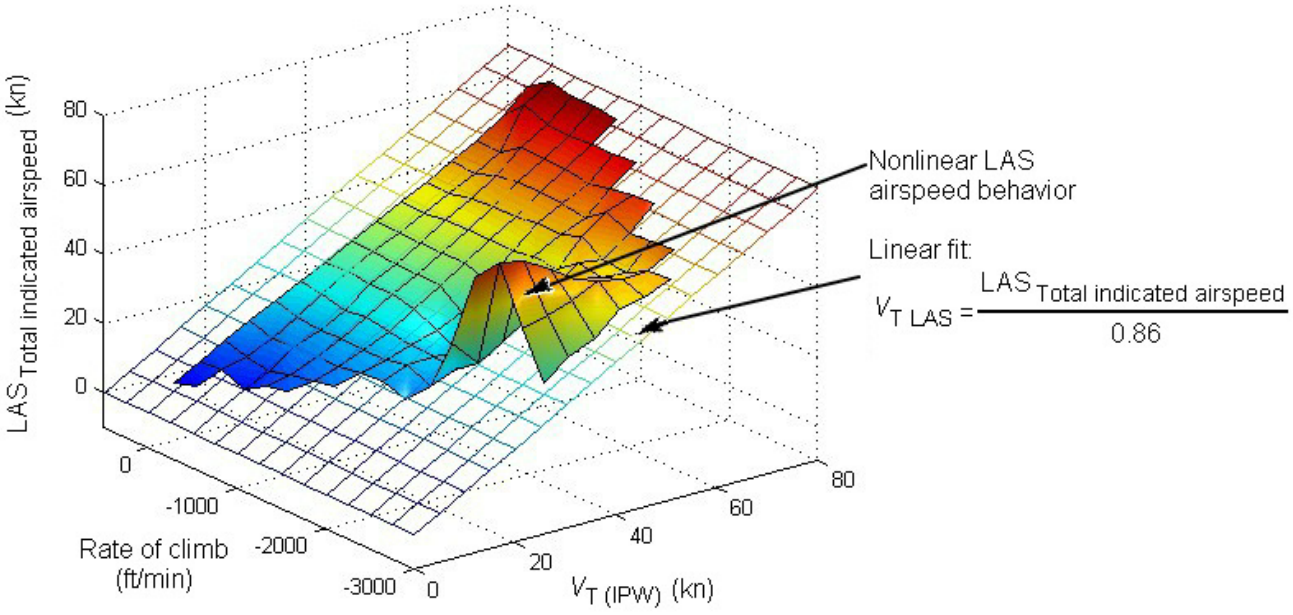

Fig. 6. Calibration indicates that the LAS behavior with total speed is nonlinear when the airspeed is low and ROD is relatively high (VRS effect).

Figure 8 illustrates the rotor outwash field during IGE hover. For a sufficiently low hover height, the rotor wash produces reversed flow at the LAS with the dominant flow going from aft to front. Supporting data from a typical V–22 liftoff are provided in Fig.9, which shows the LAS output during a transition from Takeoff to IGE Hover to out-of-ground-effect (OGE) hover. It was repeatedly demonstrated that during a liftoff, the V_{XLAS} reading would become negative (reverse flow). This negative speed readout in the cockpit did not cause alarm, as it was obviously not representative of the free-stream speed. The negative speed readout in IGE hover, however, did provide a sound basis for ignoring the negative V_{XLAS} when near-VRS conditions were encountered. It was reasoned that during high rates of descent, a flow pattern similar to that of IGE hover emerges. Figure 10 illustrates the conjectured flow field for near-vertical high rate of descent. The flow visualization inset from Drees (Ref. 1) supports the notion that a roughly toroidal flow pattern emerges when the rotor approaches VRS conditions. The LAS, being located in front of the airframe, would become immersed in a locally reversed flowfield in VRS conditions. The measured flow reversal during an actual VRS condition is shown in Fig. 11a, which illustrates a time-history of a low-speed/HROD descent encountering fully developed VRS conditions.

In Figs. 11 a and 11b, it is seen that as the rate of descent approaches 2000 ft/min (near time = 1550), the V_{XLAS}

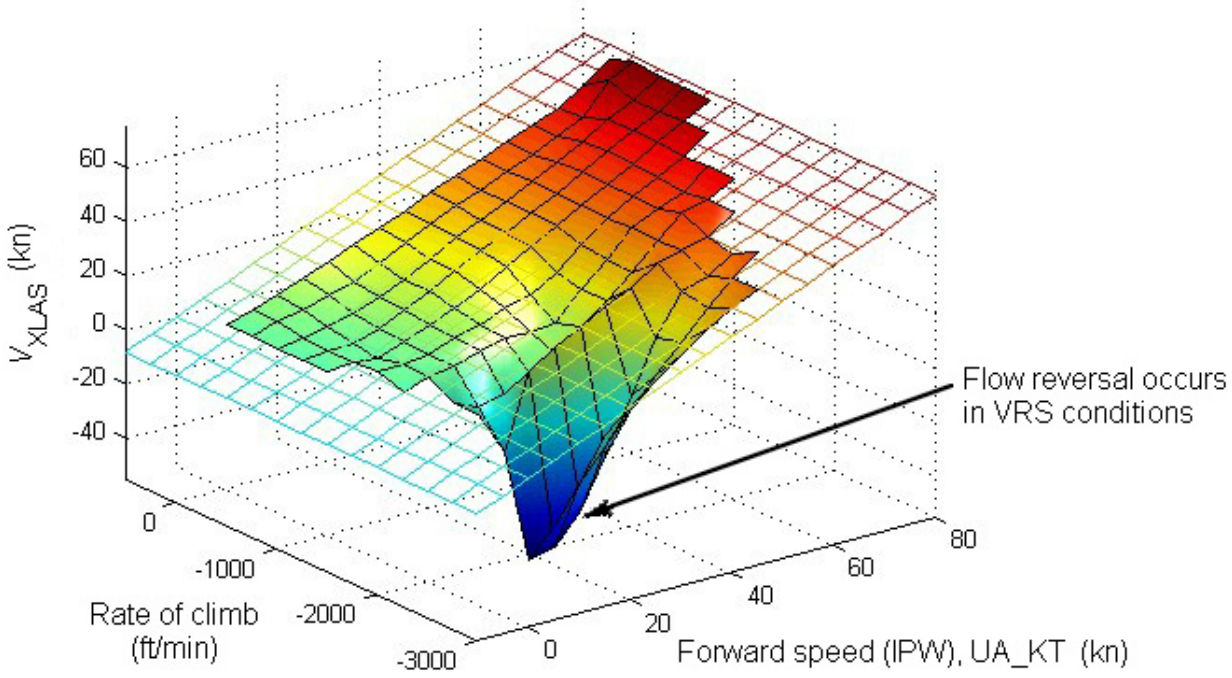

Fig. 7. V_{XLAS} behavior shows large reverse flow at the LAS during VRS encounters, even though the aircraft is moving forward through the air mass.

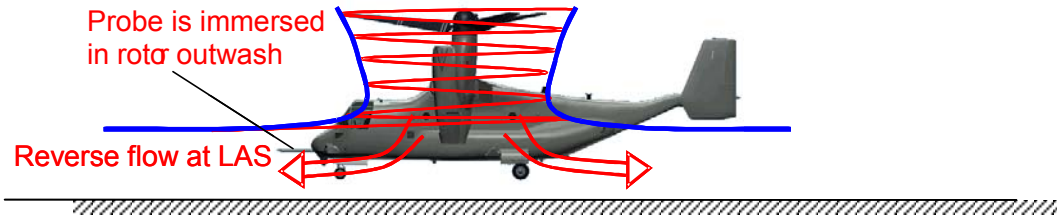

Fig. 8. Negative V_{XLAS} readings are observed while hovering in ground effect.

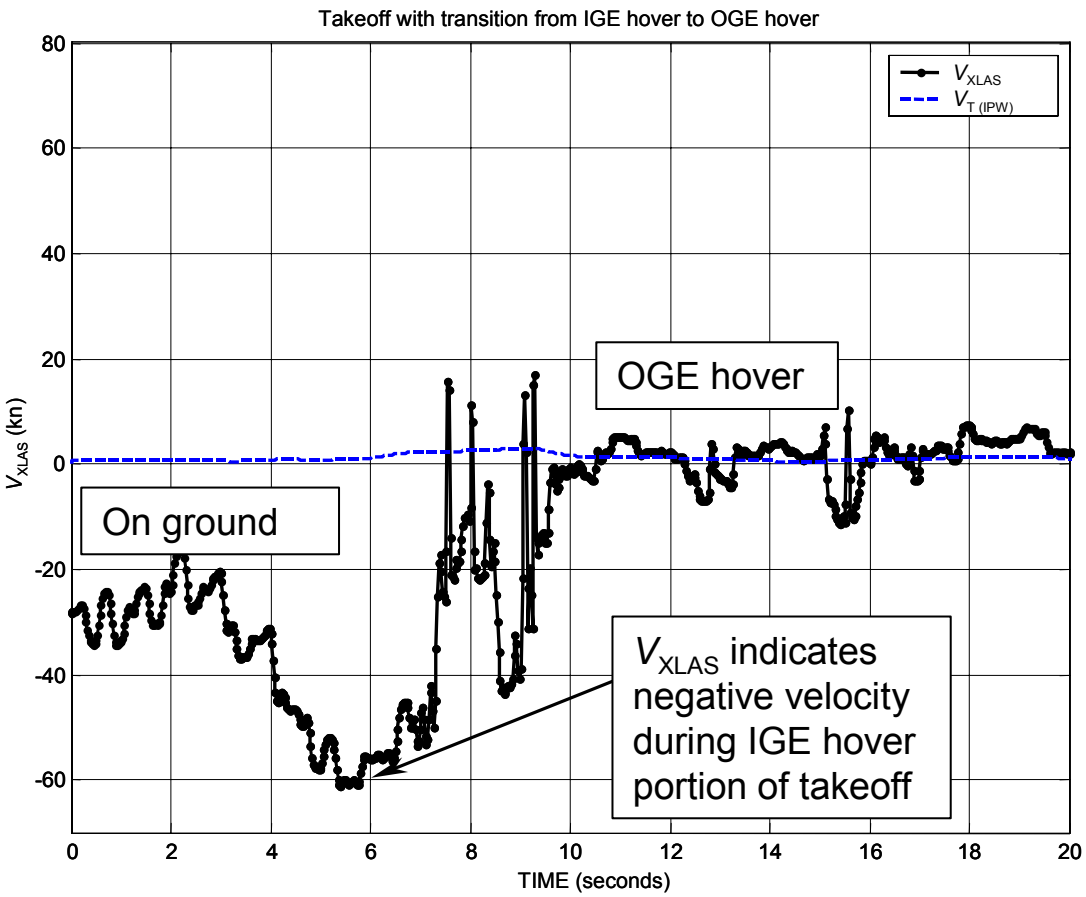

Fig. 9. During IGE hover, V_{XLAS} goes negative due to rotor outwash.

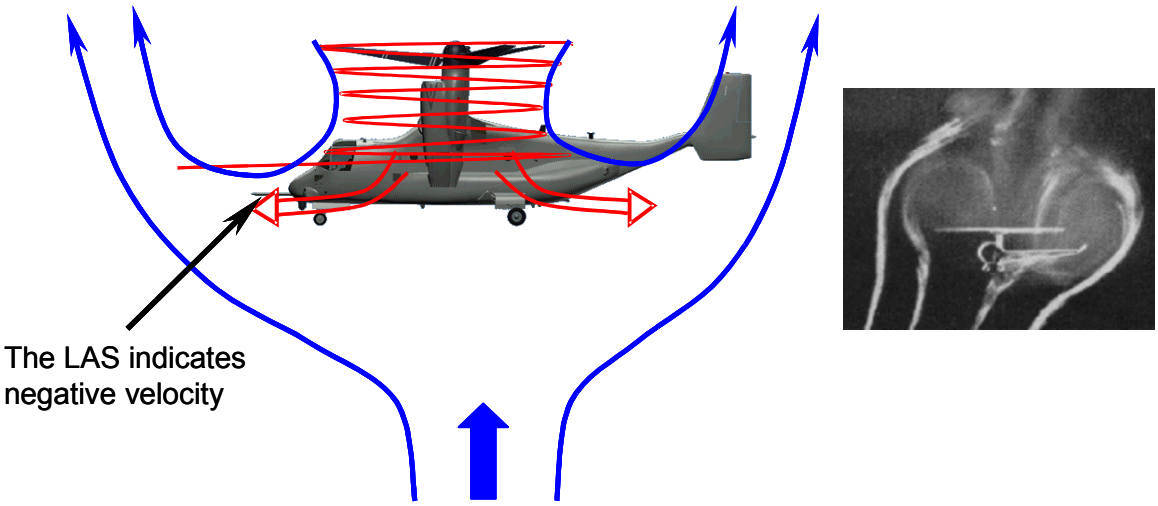

Fig. 10. In low forward speed HROD conditions, the V_{XLAS} component reads negative velocities that are associated with local flow reversal due to the rotor wake flow interaction with the onset flow. (Inset from Drees, Ref. 1)

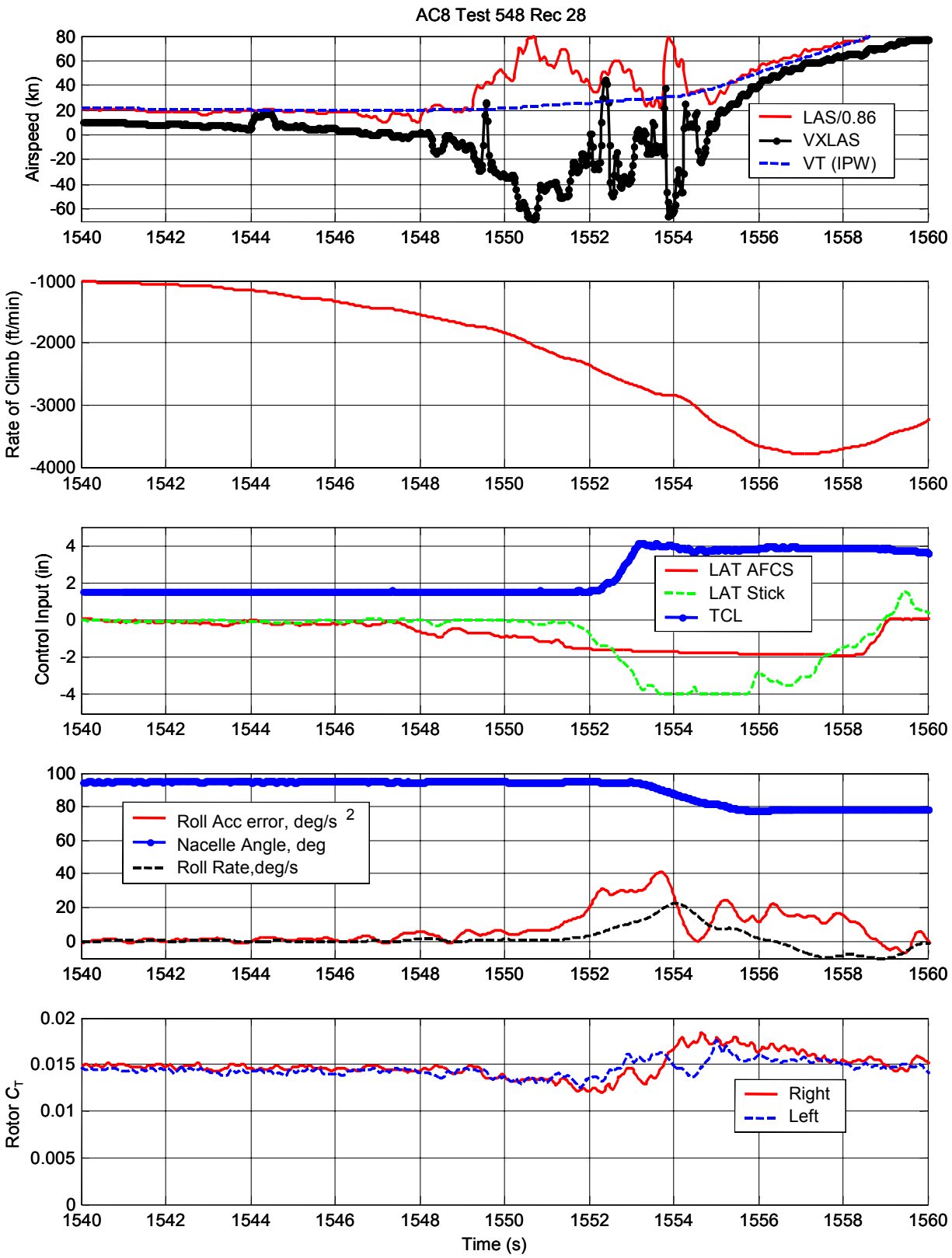

Fig. 11. A VRS encournter: HROD data at low forward airspeed.

component becomes negative, even while the true airspeed is approximately 20 kn. The pattern is nearly identical in magnitude to the negative V_{XLAS} velocities observed in the IGE hover data of Fig. 9, supporting the conjecture that the HROD flow pattern depicted in Fig. 10 is the correct one. In low speed/HROD, this type of LAS signal was recognized as a repeatable indicator of VRS. The analogy to IGE hover provided reasonable evidence that the aircraft was not flying backward at a high rate of descent and allowed testing to proceed to the lower forward speeds in spite of negative V_{XLAS} readings in the cockpit. It also became obvious that a negative V_{XLAS} reading was only one of several identifiers that, if ignored, would lead to more severe VRS symptoms, including uncommanded roll. Figs. 11c through 11e are discussed in the next section.

PARAMETERS THAT IDENTIFY VRS

Rotor Thrust Deficit

The V–22's rotor yoke is instrumented to measure bending moments caused by blade lift. Extensive correlation with flight test data provides a database for determining rotor thrust as a function of the combined yoke beam bending gauges for all blades, and both rotors. As a result, the V–22 rotor thrust can be measured with fair accuracy throughout the low-speed/HROD envelope. With numerous long record files available throughout the low-speed/HROD envelope (Fig. 4), it is possible to identify in-flight parameters that indicate VRS severity, and map them directly to the HROD envelope. Thrust is one of these parameters. For an isolated rotor, VRS is manifested (in a time averaged sense) as a reduced ability to generate thrust at a fixed collective. Betzina's data (Ref. 5) showed that a large collective pitch increase would be necessary to maintain thrust in deep VRS conditions. At the same time, VRS is an unsteady phenomenon, associated with fluctuations in thrust over time. For impending VRS, it is unlikely that two adjacent rotors would simultaneously experience identical sustained thrust deficits. In the case of tiltrotors, the side-by-side rotor configuration makes it clear that VRS symptoms will be manifested by asymmetry in the lateral control axis. Asymmetry occurs when one or the other rotor first manifests what is here called a "latent thrust deficit". A latent thrust deficit means that one or the other rotor is operating at a higher collective pitch to equalize its thrust relative to the opposite rotor. During VRS buildup, thrust oscillations appear on both rotors; sometimes they are in-phase (left and right rotors both sense a fluctuation), and sometimes they are not. The important concept for tiltrotors in VRS is that the average thrust of both rotors remains equal as long as adequate control margin is available. The primary effect of impending VRS is therefore a developing collective pitch asymmetry during an otherwise wings-level trim condition. For the tiltrotor, thrust equalization is achieved by the lateral control axis, which is described in the next section.

In addition to latent thrust deficit on one rotor, both rotors experience some actual thrust deficit during fully developed VRS, because collective pitch is held constant for most of the maneuver. For the example shown in Fig. 11e, the thrust of both rotors is approximately $C_T = 0.015$ at the start of VRS, and is reduced to approximately $C_T = 0.013$, just prior to the pilot's collective (TCL) input near time ~ 1552 seconds. It is seen, however, that the thrust on both rotors increases after the TCL input (shown in Fig. 11c), perhaps confirming Betzina's observation (Ref. 5) that the rotor thrust (in VRS) maintains a positive relation (albeit of reduced slope) with collective pitch. As a general caution to others researching VRS, it is important to note that the dynamics of VRS in a maneuvering rotorcraft may produce observations that are substantially different from steady state VRS experiments carried out in a wind tunnel, or by analysis. A VRS-induced thrust loss does not change the relative descent rate (wind) in a wind tunnel test. In flight test, however, a thrust loss must result in an increased sink rate, with attendant growth of VRS. If the dynamics of VRS buildup take away thrust more rapidly or to a greater extent than the collective pitch can restore, it may be reasoned that a pilot would report collective pitch as being ineffective in providing additional thrust during VRS. Regardless of this, the data in Fig. 11e should serve to emphasize that VRS is a high thrust event, as discussed later in the theoretical analysis section.

Lateral AFCS Output Signal

The V–22 lateral axis is controlled by both a Primary and an Automatic Flight Control System (PFCS and AFCS). The purpose of the AFCS is to improve the handling qualities of the aircraft throughout the flight envelope. However, the AFCS has a limited authority over the PFCS. The PFCS provides the pilot with $\pm$4 inches of lateral stick authority. Within the $\pm$4 inch total lateral control range, the lateral AFCS can provide up to 2 inches of equivalent lateral stick input in VTOL mode flight. For HROD configurations (VTOL Mode), the lateral stick primarily controls the rotor differential collective pitch (DCP), which relates directly to the commanded thrust difference between the two rotors. For a left stick input, DCP increases the collective pitch of the right rotor, and decreases the collective on the left. When a lateral thrust asymmetry is first encountered, the AFCS will automatically apply lateral control to compensate for the roll disturbance, and thereby reduce pilot workload. During VRS buildup, high levels of offset in the lateral AFCS output are an indicator of VRS-induced asymmetry in the lateral control axis. Referring again to the VRS event of Fig. 11, subplot c shows that the lateral AFCS begins to

apply an equivalent left lateral stick input when the rate of descent is near 1,500 ft/min (458 m/min). As descent rate continues to increase (Fig. 11b), the degree of VRS increases. In this example, the right hand rotor is experiencing a latent thrust deficit relative to the left rotor, as evidenced by the growing lateral AFCS output. The lateral AFCS is increasing the collective pitch of the right rotor to compensate for the VRS-induced latent thrust asymmetry, and keeps the wings level without pilot (lateral stick) intervention.

As the descent rate continues to increase, the lateral AFCS runs out of authority just prior to time 1552 in Fig. 11c[2]. As seen in Fig. 11d and 11c, the pilot detects the aircraft rolling right and applies left stick input through the PFCS near time ~ 1552 seconds. However, the descent rate is so high, and VRS so developed that the full lateral stick input does not prevent roll, and a recovery with nacelle tilt is initiated near time = 1553. Throughout the developing VRS, it is seen that once a latent thrust deficit is manifested in a given rotor, that rotor will require a higher collective pitch for the duration of the encounter (until recovery by nacelle tilt). A key observation for VRS is that in no case does the latent thrust deficit appear to alternate between rotors once an asymmetry develops. The act of increasing the collective pitch on the "low-thrust" right rotor and decreasing the collective pitch on the "high-thrust" left rotor (through the lateral control axis) equalizes the rotor thrust during VRS buildup, but it also results in furthering the latent thrust deficit in the "deficit rotor." Without an intervening recovery, the aircraft will experience an uncommanded roll in the direction of the rotor that first experienced a thrust deficit, even if the deficit occurred early in the maneuver. This observation indicates that the rotor with a growing latent thrust deficit will enter fully developed VRS before the "lower collective" opposite rotor.

In Fig.11d, the pilot recovers from VRS by applying forward nacelle tilt near time ~ 1553 seconds. It is seen that the VRS-induced roll rate (due to the thrust asymmetry) begins to recover within one second after the pilot-initiated nacelle tilt. In every case, nacelle rotation was a reliable and rapid method for releasing the rotors from VRS and for resuming the test.

By examining the lateral AFCS output for all HROD data (in Fig. 4) it is possible to directly map both the scope and the severity of VRS symptoms over the entire flight envelope. Using the long-record time history files of Fig. 4, the magnitude of the lateral AFCS output is extracted and shown as a contour plot in Fig. 12. While lateral AFCS output can occur anywhere in the flight envelope (due to maneuvers/control inputs), most of the time history data of Fig. 4 represents quasi-steady state flight conditions, where relatively little AFCS activity would be anticipated. Nevertheless, portions of the data are affected by control inputs while maneuvering to target conditions, and do not represent VRS-induced offset. Control input-related AFCS output explains small anomalies in the lateral AFCS signal in otherwise smooth regions of the HROD envelope. Any given point in the contour map represents the average magnitude of the AFCS output signal for all flight test data within the surrounding region. Figure 12 clearly shows the location of VRS as detected by the lateral AFCS signal. For steady rates of descent near 1,800 ft/min (549 m/min) (in the 20 knot speed range), the average lateral AFCS output ranges up to about 0.8 inch of equivalent lateral stick input (on the basis of averaging many individual points in the long record files). Inside a boundary roughly identified by the 0.8 inch contour line, VRS can be expected to be fully developed and the full authority of the lateral AFCS and the pilot PFCS command may be required to prevent an uncommanded roll. The long record analysis method provides a general approach for identifying the location of the VRS boundary by examining all available test data. The contour plot represents over 31,000 data points accumulated at ½-second intervals over the entire HROD envelope.

Roll Acceleration Error

While thrust fluctuations and degraded thrust control are primary indicators of VRS in helicopters, it is seen that degraded lateral control authority is the primary indicator of VRS in tiltrotors. When the lateral AFCS port output goes high, the pilot will invariably begin exercising additional lateral control through the primary flight control system, as Fig 11 showed. The sum of the lateral AFCS and lateral PFCS will command differential collective pitch (DCP) between the left and right rotor systems. In normal VTOL mode flight conditions, DCP produces differential thrust between the rotors, generating a rolling moment about the aircraft cg. The corresponding roll acceleration is approximated by a linear relationship with DCP. If the expected roll acceleration for a given DCP does not emerge, it is because the thrust on one or both rotors is being affected by VRS. The roll acceleration error is defined as the difference between the expected roll rate and what was actually measured. In otherwise steady flight conditions, the roll acceleration error at once provides an expression for the severity of VRS that considers the expectations of both the pilot, and the automatic flight control system. Put simply, the roll acceleration error term is a direct measure of the ability of the lateral control system to generate roll acceleration. When the pilot (or AFCS) applies lateral control, roll acceleration in the corresponding direction is the desired result. Since VRS interferes with thrust, roll acceleration

[2] Note: Time constants built into the control laws delay the full 2-inch AFCS input until time = 1558.

VRS interferes with thrust, roll acceleration errors will become evident as VRS conditions worsen. Referring back to Fig. 11d, it is seen that the roll acceleration error grows rapidly as the rotor descends into fully developed VRS. By the time the pilot commands full (4-inch) left stick (in Fig. 11c at time ~1,553.5 seconds), the fully developed VRS on the right rotor produces a thrust deficit large enough that an uncommanded right roll ensues. The roll acceleration error in Fig. 11d is large because a right roll occurs in spite of a full left stick input. Using the contiguous long record data, the roll acceleration error (magnitude) for all HROD test points in Fig. 4 are calculated and mapped to the HROD flight envelope. The result is expressed as a contour diagram of the average magnitude of the roll acceleration error for all descent rates and forward speeds, as shown in Fig. 13.

Together, Figs. 12 and 13 show that the lateral control axis is strongly affected by VRS. In severe VRS conditions the lateral AFCS signal will saturate, as its full authority is demanded to maintain a wings-level condition. Figure 13 substantiates the region where a pilot will encounter VRS and indicates the degree of decreasing lateral control margin as roll acceleration errors compound with increasing descent rate in the low speed regime. For VRS, the quality and ultimate limits of controlled flight are identified by the contours in Figs. 12 and 13. When the aircraft proceeds to cross deeply into the contours, a departure from controlled flight can be anticipated in the form of an uncommanded roll. The contours in Fig. 13 are predictors of the severity of the latent thrust deficits and uncommanded roll. For low contour values, the AFCS will correct them. For moderately higher

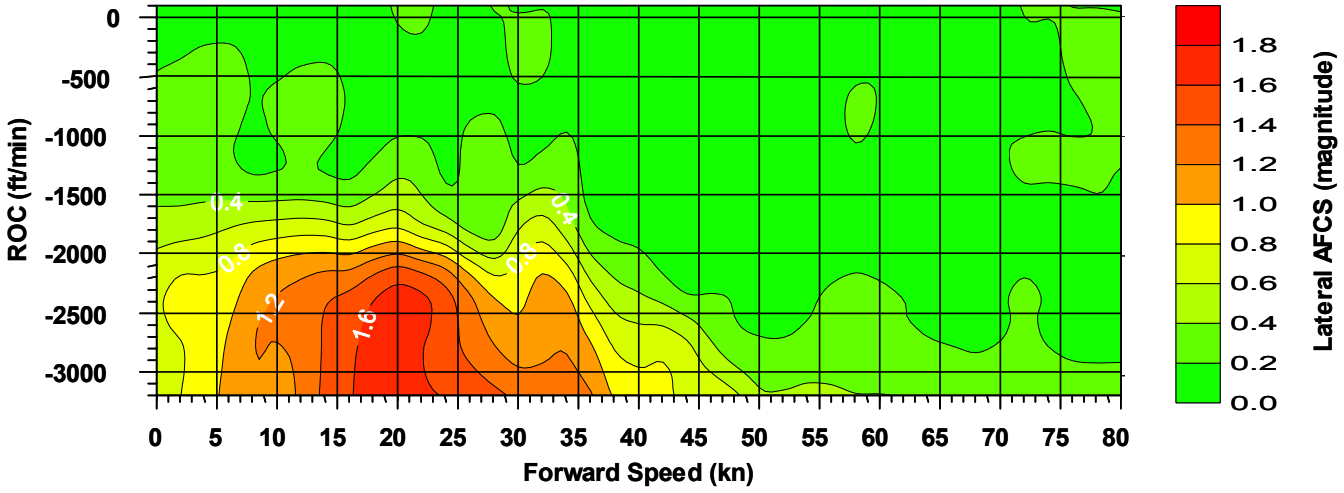

Fig. 12. Lateral AFCS port output in otherwise steady flight conditions is a good indicator of the severity of VRS.

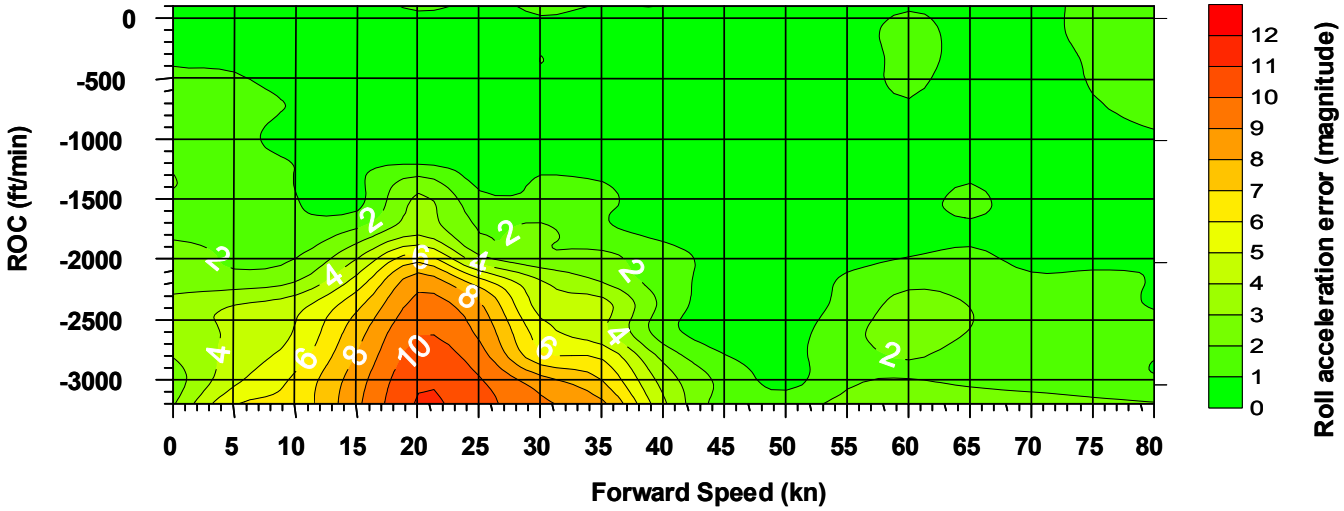

Fig. 13. Mean roll acceleration error indicates control asymmetry as a symptom of VRS.

contour values, the pilot enters the loop and may be able to control the roll acceleration errors with sufficient lateral stick input. For high contour values, even the full lateral authority of the PFCS will not arrest the roll rate, and a recovery (forward nacelle tilt) will be required to re-establish roll control.

It is worth returning to Fig. 11d to note a subtle difference between the lateral AFCS output and roll acceleration error in VRS. The lateral AFCS detects VRS, but cannot keep up with rapid changes in rotor thrust when VRS is fully developed. As a VRS indicator, the lateral AFCS approaches saturation while symptoms are still increasing. The roll acceleration error, on the other hand, shows the gradual rise in VRS symptoms early on, but also shows the precipitous nature of fully developed VRS well after the pilot applies full left stick. Figure 11d shows the roll acceleration error increasing dramatically shortly after the pilot left stick input. Betzina's observation (Ref. 5) that a large collective pitch increase is required just to maintain thrust in deep VRS conditions means that if additional collective pitch is not available (through the DCP command), the latent thrust deficit of one rotor will become actualized very suddenly and, in fully developed VRS, an uncommanded roll rate will emerge (as shown in Fig. 11 d) unless recovery is initiated.

Comparison with thrust fluctuations

In Ref. 9, Kisor et al. develops a chart showing the magnitude of rotor thrust oscillations based on individual test records near the VRS boundary. Different boundaries are drawn, depending on the severity of thrust fluctuations and asymmetries. Figure 14 represents Ref. 9 data expressed in dimensional units and superimposed upon the roll acceleration error plot of Fig. 13. Although Ref. 9 data is derived independently, from individual test points, it is evident that the results harmonize with the contiguous long record analysis and substantiate the boundaries of VRS for the V–22. In Fig. 14, the "thrust fluctuation" and "asymmetry" boundaries represent regions where the thrust disturbances increase linearly. Latent thrust asymmetries grow in this region, but remain controllable by AFCS and PFCS commands. As the onset boundary is approached, the gradient of roll acceleration error becomes markedly steeper. This boundary is identified in Ref. 9 as a region where the rotor response to collective pitch is dramatically different. Much higher collective pitch is required to maintain thrust in the "onset region," a trend that was also identified by Betzina in Ref. 5. The onset boundary represents the condition where uncommanded roll may be expected under steady descent conditions. Kisor (Ref. 9) shows that this region of VRS symptoms also coincides with dramatic changes to the yoke chordwise bending loads. The loads become constant with azimuth, indicating that the blades are in an axially symmetric flowfield, consistent with the toroidal flow often depicted for VRS (see Fig. 10 inset). Individual test records identifying uncommanded rolloffs are shown as triangular data points in Fig. 14.

Comparison with Theory

As mentioned in the introduction, extensions to simple momentum theory have been developed to identify the VRS boundary. While simple momentum theory is strictly not valid for VRS conditions, due to loss of an identifiable stream tube, the limit can be probed using methods such as

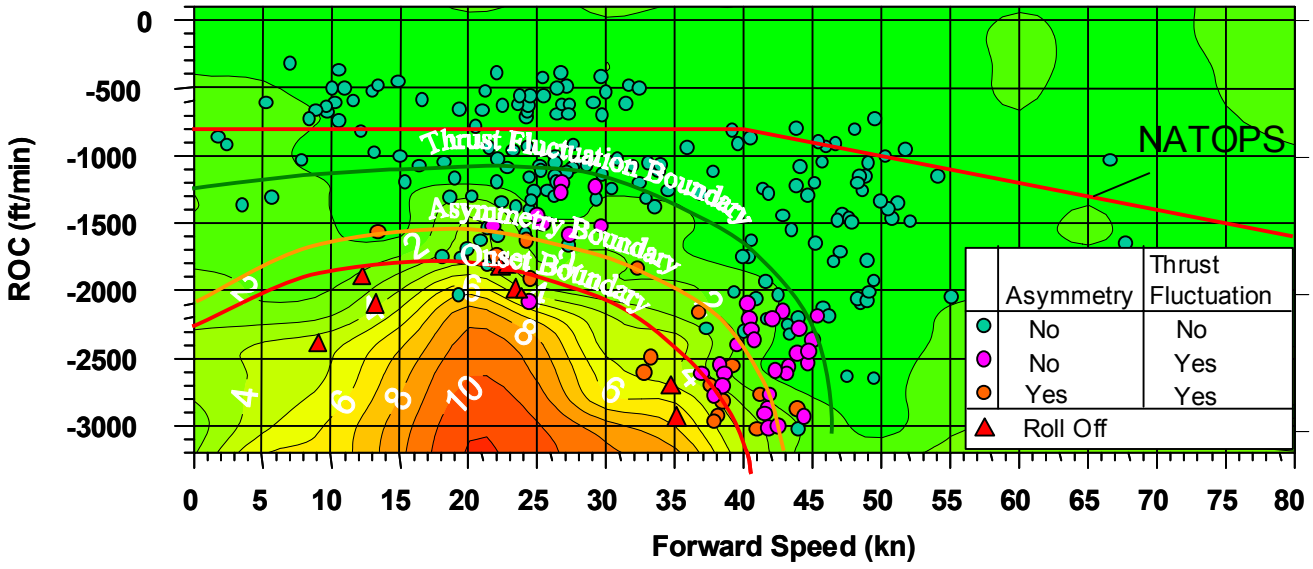

Fig. 14. Supporting test data and the associated VRS boundaries from Ref. 9 shown superimposed on the roll acceleration error contours demonstrates consistent results with the long record analysis method.

the one developed by Newman et al. in Ref. 7. This method provides a useful engineering tool for assessing the effects of thrust and rotor tip speed on VRS. In Ref. 7, Newman et al. develop a wake transport criterion for assessing VRS conditions. The wake transport velocity consists of the vector sum of forward speed, climb (descent) speed, and the rotor induced velocity at the tip path plane. The wake transport velocity components tend to separate the tip vortex filaments. Inflow and climb speed provide vertical separation, while forward speed provides some horizontal separation. Therefore, Newman et al. developed the "effective" wake transport velocity term:

$$\bar{\mu}_{\text{Effective Wake Transport Velocity}} = \sqrt{\left(k\ \ \bar{\mu}_x\right)^2 + \left(\bar{\mu}_z + \bar{\lambda}_i\right)^2} \quad (1)$$

In Ref 7, a calculation was put forward, indicating that the forward speed component $\bar{\mu}_x$ was only 63.6% as effective (as inflow, or climb rate) in providing tip vortex filament separation. Nevertheless, Newman et al. (Ref. 7) indicated that assigning a value of k = 0.65 gave better correlation with experimental data. The authors went on to theorize that when the effective wake transport velocity term (above) is less than a certain "critical" value, the rotor wake vortex filaments would tend toward accumulating near the rotor disk, rather than convecting away. If the aggregate accumulation of vorticity, produced by the rotor blades, could not convect away from the rotor, an unstable air mass formed near the rotor, leading to the symptoms of VRS.

Continuing the analysis of Ref. 7, Newman et al. showed that the boundary for the onset of wake flow breakdown was given by the following expression:

$$\bar{\mu}_z = \sqrt{\bar{\mu}^2_{\text{Critical Effective Wake Transport Velocity}} - (0.65\ \ \bar{\mu}_x)^2} - \bar{\lambda}_i \quad (2)$$

$$\text{where } \bar{\lambda}_i = \frac{1}{\sqrt{\bar{\mu}_x{}^2 + (\bar{\mu}_z{}^2 + \bar{\lambda}_i)^2}} \text{ and}$$

$$\bar{\mu}_{\text{ Critical Effective Wake Transport Velocity}} = 0.74$$

Newman et al. (Ref 7) selected the value (0.74) for the critical velocity on the basis of matching experimental observations from the flow visualization of Drees and Hendal (Ref. 1).

Solving the above expressions[3] for wake flow breakdown leads to the predicted VRS boundary curve shown in Fig. 15. The curve represents the predicted non-dimensional descent rate and forward speed, where VRS may be encountered.

Using parameters derived from the V–22 flight test data, the non-dimensional data in Fig. 15 can be expressed in dimensional units. As stated earlier, the V–22 rotor thrust is known throughout HROD testing from calibrations of the yoke–beam-bending gauges. Although HROD testing typically occurs at relatively low collective pitch, it should be pointed out that VRS onset conditions actually occur at approximately 1*g* normal load factor, and therefore VRS is a high thrust event (as was shown in Fig. 11d). Forward speed is too low for the V–22 wing to provide any substantial lift. For the low-speed/HROD test data of Fig. 4, the average V–22 rotor thrust coefficient was approximately C_T = 0.016. The mean thrust was reduced only when VRS symptoms became severe and rolloff/recovery was initiated. Regardless, the thrust coefficient rarely dropped below C_T = 0.014, and rarely exceeded C_T = 0.018. Variations in thrust coefficient were primarily due to altitude changes (temperature change during a test), or temperature changes with daily weather, or gross weight variations due to fuel burn. In this respect, the V–22 flight test data are different from certain wind tunnel data, and certain analyses. The flight test data represent trimmed rotor conditions at a high (mean) thrust throughout the test point setup and relatively far into the VRS condition. When comparative VRS wind tunnel data are examined, or VRS analyses are performed, the high thrust condition must be accounted for because, as the simple engineering analysis shows next, VRS boundaries are dependent on thrust. These situations are pointed out because they can be, and have been, issues in describing VRS susceptibility for highly twisted rotors (Ref. 11). Using the typical V–22 range of flight test thrust coefficients, and the

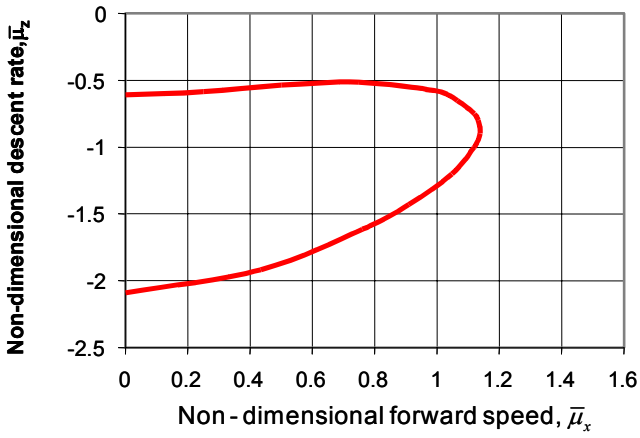

Fig. 15. Analytical prediction of the VRS boundary, with speeds normalized by hover-induced velocity (Ref. 7 theory with k = 0.65, $\bar{\mu}_{\text{critical effective wake transport velocity}} = 0.74$).

[3] The solution process, being iterative in nature is somewhat lengthy, and is out of the scope of the present paper.

nominal rotor tip speed of 790 ft/s (241 m/s), Fig. 16 expresses the predicted VRS boundary in dimensional form.

The engineering model supports the generally accepted result that higher thrust will allow higher rates of descent before VRS symptoms are encountered. It also predicts that higher thrust will extend the VRS boundary to higher forward airspeeds. The theoretical VRS boundary is compared to the Roll Acceleration Error, and the boundaries developed by Kisor et al. (Ref. 9) in Fig. 17.

The theoretically derived VRS boundary in Fig. 17 is based on numerical parameters (identified by Newman, Ref. 7) to empirically match visualizations of rotor wake data in Ref. 1. Assuming that the theoretical boundary applies to the V–22 roll-off boundary, it is seen that the engineering model is overly conservative (by approximately 6 kn) in terms of defining the forward speed VRS boundary, and optimistic (by approximately 370 ft/min [113 m/min]) in terms of defining the descent rate for encountering VRS at low speed. Analysis indicates that the horizontal limits of the boundary curves in Fig. 16 are somewhat sensitive to the value selected for the parameter k, and better correlation may be achieved if a slightly higher value is used. This indicates that the effectiveness of forward speed in dispersing vortex filaments may be somewhat higher than theorized by Newman (k = 0.65). The 370 ft/min (113 m/min) discrepancy in predicting the descent rate for VRS onset may serve to indicate that rotor inflow is not 100% effective in providing vortex filament separation either, and a separate "k_2-factor" could be applied to this term of the wake transport equation as shown below:

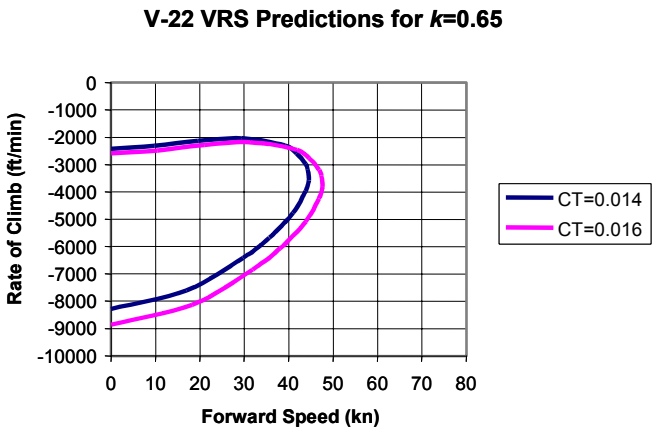

Fig. 16. Predicted dimensional VRS boundary for V–22 parameters, based on engineering model by Newman et al. (Ref. 7), with parameters selected from Drees (Ref. 1) flow visualization observations.

$$\bar{\mu}_{\text{Effective Wake Transport Velocity}} = \sqrt{(k\bar{\mu}_x)^2 + k_2{}^2(\bar{\mu}_z + \bar{\lambda}_i)^2} \quad (3)$$

Nevertheless, the basic prediction indicates that the simple engineering model captures the general vicinity of measured VRS activity for the V–22 and therefore serves to preclude the notion that the V–22's unique design is not amenable to analyses that work for conventional helicopters. In particular, the V–22's side-by-side rotor configuration and high blade twist do not lead to a VRS susceptibility that is out of line with simple engineering theory. The result shows that the V–22's higher disk loading is the single main factor in defining its VRS boundary. Therefore, when more sophisticated prediction methods are employed to predict the V–22's VRS susceptibility, they must recognize the V–22's

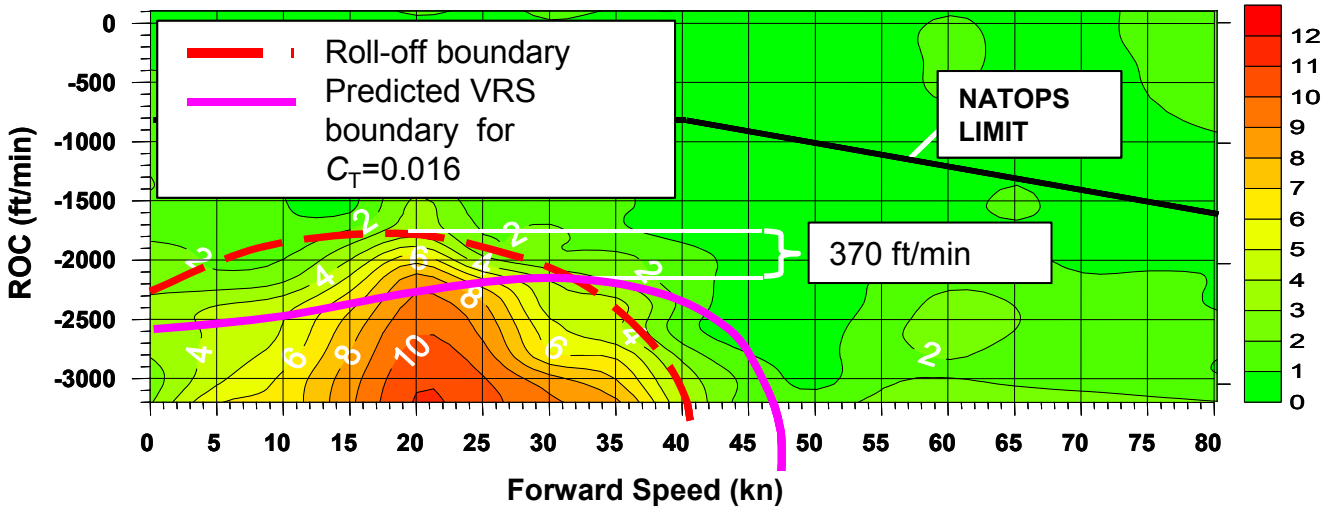

Fig. 17. The theoretical VRS boundary for C_T = 0.016 (using Ref. 7 formulation).

high disk loading and utilize representative thrust coefficients (near C_T=0.016), or a very spurious result could be reported.

CONCLUSIONS

The V–22 ITT has completed Vortex Ring State testing for the V–22. The results for quasi-steady state descent rates are presented, and dynamic maneuvers are discussed with the following conclusions:

1. In conjunction with proper test procedures that utilize wind collection and inertial reference data, long record analysis can be used to calibrate airspeed sensors for use in low-speed/high rate of descent testing.

2. The long record process provides a semi-automated method for extracting HROD test data from an entire flight, without the need to identify specific test records and events. Since the data records are contiguous, an entire map is developed to show the full extent and severity of VRS throughout the descending flight envelope.

The V–22 testing has shown the following:

1. In fully developed VRS, the V–22 exhibits lateral control asymmetry, followed by uncommanded roll rate.

2. The initiation of forward nacelle tilt rapidly restores lateral control allowing flight out of the VRS boundary and releasing the rotors from VRS.

3. At low forward speed and increasing descent rate, VRS will be accompanied by increasingly higher output in the lateral control axis. This is because VRS interferes with rotor thrust, and produces a collective pitch asymmetry between the left and right hand rotors. Higher lateral AFCS port output is confined to airspeeds below approximately 45 kn, when the descent rate is higher than 1,500 ft/min (458 m/min).

4. The high lateral AFCS output region correlates with another lateral axis parameter, called the roll acceleration error. The roll acceleration error, identified by long record analysis, substantiates the independently derived VRS boundaries of Kisor et al. (Ref. 9).

5. The VRS boundary defined in steady descent testing defines the most conservative boundary for encountering VRS symptoms. Control inputs, including yaw rate, roll rate, and rapid deceleration all tend to suppress/delay VRS symptoms. It was not possible to initiate VRS symptoms outside of the static VRS boundary during any dynamic maneuver (Ref 9).

6. Reasonable correlation to the measured V–22 VRS boundary is achieved by the simple engineering analysis of Newman et al. (Ref. 7) by properly accounting for the V–22's high rotor disk loading (thrust). The correlation achieved between measurements and the analysis demonstrates that the primary factor in determining the V–22 VRS boundary is disk loading, not blade twist, nor blade planform, nor side-by-side rotor interference.

7. In comparison to the published NATOPS descent rate limitation, it is shown that the V–22 has significant margin for avoiding VRS.

ACKNOWLEDGMENTS

The authors gratefully acknowledge the efforts of Mr. Anura Senanayake (Boeing), Mr. Stanley Briczinski (Boeing), and Mr. Domenico Alvaro (Bell), for their assistance in processing numerous test records to verify kinematic consistency of the data, and generate the numerous long record history files with wind aloft predictions. All tests were conducted at the Patuxent River Naval Air Station, with the support of numerous ITT members, including Bell, Boeing and NAVAIR engineering. The focus of Mr. Ray King (Boeing Flight Test Director) and guidance of Mr. Jay Samak (Bell V–22 Technology Lead) assured that the test objectives were achieved with each flight. At last, the test pilots Tom Macdonald (Boeing), Steve Grohsmeyer (Boeing), and Bill Leonard (Bell Helicopter) deserve special mention. They ventured into an unexplored flight regime, providing a continuous data stream to mark this new territory.

REFERENCES

1. Drees, J. M., and Hendal, W.P., "The Field of Flow Through a Helicopter Rotor Obtained from Wind Tunnel Smoke Tests," *Journal of Aircraft Engineering*, Vol. 23, (266), pp. 107–111.

2. Yaggy, P. and Mort, K. "Wind Tunnel Tests of Two VTOL Propellers in Descent," NASA TN D-1766, March 1963.

3. Washizu, K., Azuma, A., Koo, J., and Oka, T., "Experiments on a Model Helicopter Rotor Operating in the Vortex Ring State," *Journal of Aircraft*, Vol. 3, (3), May-June 1966.

4. Johnson, Wayne, “Model for Vortex Ring State Influence on Rotorcraft Flight Dynamics,” American Helicopter Society 4th Decennial Specialist’s Conference on Aeromechanics, San Francisco, CA, January 2004.

5. Betzina, Mark D., “Tiltrotor Descent Aerodynamics: A Small-Scale Experimental Investigation of Vortex Ring State,” American Helicopter Society 57th Annual Forum, Washington, DC, May 2001

6. Wolkovitch, J., “Analytical Predictions of Vortex Ring Boundaries for Helicopters in Steep Descents,” *Journal of the American Helicopter Society*, Vol. 17, 1972.

7. Newman, S., Brown, R., Perry, J., Lewis, S., Orchard, M., and Modha, A., “Predicting the Onset of Wake Breakdown for Rotors in Descending Flight,” *Journal of the American Helicopter Society*, Vol. 48 (1), Jan. 2003.

8. Taghizad, A., Jimenez, J., Binet, L., and Heuze, D., “Experimental and Theoretical Investigations to develop a model of Rotor Aerodynamics adapted to Steep Descents,” American Helicopter Society 58th Annual Forum, Montreal Canada, June 2002

9. Kisor, R., Blyth, R., Brand, A., and Macdonald, T., “V–22 Low Speed/High Rate of Descent Test Results,” American Helicopter Society 60th Annual Forum, Baltimore, MD, June 2004.

10. Kearney, S. and Lake, R., “Low Airspeed Sensor,” American Helicopter Society 59th Annual Forum, Phoenix, AZ, May 2003

11. Brown, R. E., Leishman, J. G., Newman, S. J., and Perry, F. J., “Blade Twist Effects on Rotor Behavior in the Vortex Ring State,” European Rotorcraft Forum, Bristol, UK, September 2002.